High Harmonic Spectroscopy of Multichannel Dynamics in Strong-Field Ionization

Y. Mairesse,[1] J. Higuet,[1] N. Dudovich,[2] D. Shafir,[2] B. Fabre,[1] E. Mével,[1] E. Constant,[1] S. Patchkovskii,[3] Z. Walters,[4] M. Yu. Ivanov,[5] and O. Smirnova[4]

[1]*CELIA, Université Bordeaux 1, UMR5107 (CNRS, Bordeaux 1, CEA), 351 Cours de la Libération, 33405 Talence, France*
[2]*Department of Physics of Complex Systems, Weizmann Institute of Science, Rehovot 76100, Israel*
[3]*National Research Council, 100 Sussex Drive, Ottawa, Ontario K1A 0R6, Canada*
[4]*Max-Born Institute, Max-Born-Strasse 2A, D-12489 Berlin, Germany*
[5]*Department of Physics, Imperial College London, SW7 2AZ London United Kingdom*

(Received 14 December 2009; published 24 May 2010; corrected 25 May 2010)

We perform high harmonic generation spectroscopy of aligned nitrogen molecules to characterize the attosecond dynamics of multielectron rearrangement during strong-field ionization. We use the spectrum and ellipticity of the harmonic light to reconstruct the relative phase between different ionization continua participating in the ionization, and thus determine the shape and location of the hole left in the molecule by strong-field ionization. Our interferometric technique uses transitions between the ionic states, induced by the laser field on the subcycle time scale.

DOI: 10.1103/PhysRevLett.104.213601 PACS numbers: 42.50.Hz, 32.80.Rm, 33.80.Wz

Nonlinear laser-molecule interaction converts incident infrared radiation into its very high harmonics. These harmonics are generated during radiative recombination of an electron liberated by strong-field ionization with the hole left in the molecule. High harmonic spectroscopy records and analyzes information about molecular structure [1,2] and attosecond dynamics [3–5], encoded in harmonic spectra, phases and polarizations.

For one-photon ionization, recent theoretical studies of core relaxation (see, e.g., [6] and references therein) predict attosecond hole dynamics [7] resulting from coherent excitation of multiple electronic states of the cation. In contrast, for absorption of multiple photons, attosecond dynamics of multielectron rearrangement during strong-field ionization is not understood. The shape and location of the hole after ionization are determined by the relative phases of the participating electronic states. Here we show that these phases, which are set up by ionization and reflect dynamics of core rearrangement, are naturally recorded in high harmonic emission. We use high harmonic spectroscopy to reconstruct these phases.

In one-photon ionization, the relative phases between ionization channels are determined by the phases of transition dipoles that couple bound and continuum states and reflect different scattering phases and orbital parity. However, photoelectron spectra do not record these phases: the ion is left in orthogonal final states, precluding interference of different continuum waves. In contrast, in high harmonic generation (HHG) different states of the ion act as different intermediate states that connect the same initial to the same final state of the system. Therefore, HHG naturally records interference of different channels, offering a route to attosecond probing of rearrangement dynamics [5]. Note, that the phase associated with strong-field ionization is fundamentally different from that familiar in one-photon ionization.

In strong-field ionization of atoms, the importance of different electronic continua arising from spin-orbit splitting of the ionic ground state was experimentally demonstrated in [8,9] and theoretically studied in [10] with the emphasis on hole dynamics. In strong-field ionization of molecules, the importance of multiple channels was pointed out in [11] and studied in detail in [5,12,13]. Pertinent theoretical work includes, e.g., [4,5,14–18].

We use high harmonic spectroscopy in N_2 molecules to reconstruct the relative phase of ionization between the two most important channels, which create the N_2^+ ion in the ground $X^2\Sigma_g$ and excited $A^2\Pi_u$ states. By analyzing the spectrum and ellipticity of the harmonic light, we show that the relative phase ϕ_{XA} between the channels X and A, imparted by ionization, approaches π for molecules aligned at $\theta \sim 50$–$90°$ from the laser polarization. In the limit of quasistatic tunnel ionization, the expected value is $\phi_{XA} \approx 0$ [5]. Deviation from the quasistatic regime in N_2 reflects the nonadiabatic character of electron rearrangement.

Our laser frequency ($\omega_L = 1.55$ eV) is close to the energy gap between these two channels ($\omega_{XA} \approx 1.3$ eV), resulting in substantial dynamics in the ion on the sublaser cycle time scale [Fig. 1(a)]. To calculate this dynamics, we calculate the field-free ionic states using the GAMESS quantum chemistry code [19], complete active space self-consistent field (CASSCF) method and correlation-consistent valence triple-zeta basis set expansion [20]. Next, we find the transition dipole moments between these field-free states and their quasistatic Stark shifts due to other states. Then, we solve the time-dependent Schröedinger equation in the restricted basis of the states X, A, B. Our initial conditions explicitly include quasistatic polarization of the ionic states at the moment of ionization: for a given ionization channel, population starts in the field-polarized ionic state. For the molecules aligned at

 © 2010 The American Physical Society

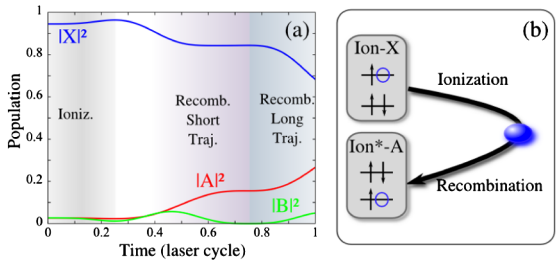

FIG. 1 (color online). (a) Subcycle dynamics in the N_2^+ ion at $\Theta = 50°$: populations of the field-free ionic states X, A, and B in a $I = 8 \times 10^{13}$ W/cm^2, $\lambda = 800$ nm laser field. (b) Cross-channel in HHG associated with real excitations induced by the laser field between ionization and recombination.

$\theta = 50°$ relative to laser polarization, the dynamics after ionization into the polarized ground X state of the ion is shown in Fig. 1(a). Note ~3% contribution of the field-free A state to the polarized X state at the peak of the field ($t = 0$).

Substantial subcycle transitions have crucial impact on harmonic radiation: when an electron, liberated, e.g., from the highest occupied molecular orbital (HOMO), returns to the parent ion, it may find the hole in the HOMO-1 orbital, Fig. 1(b). Thus, multichannel HHG includes both diagonal and off-diagonal channels i, f (i, $f = X$, A label the states of the ion after ionization, i, and before recombination, f). For example, XA channel means ionization into the (polarized) X state of the ion, excitation from the X state to the A state between ionization and recombination, and recombination with ion in the A state. Channel XA is very substantial at large alignment angles θ. Compared to XX it benefits from stronger recombination: at $\theta = 90°$ recombination to A is larger than to X, [17]. Compared to AA it benefits from stronger ionization: in our calculations, at $\theta = 90°$ ionization is ~5 times stronger for X channel than for A channel, see also [15,18]. The coupling between the X and A states is perpendicular, and the population transfer between X and A states approaches 30%–40% for $\theta = 90°$ at $I = 10^{14}$ W/cm^2. Thus, the intensity of the XA channel is about 2 times higher than that for AA channel at $\theta = 90°$. Channels associated with the B state of N_2^+, also included, are less important for $\theta \geq 50°$.

At first glance, these cross-channels might seem an unwelcome complication, but they are not. Indeed, the interference between the diagonal channels XX and AA is controlled by the relative phases of ionization, recombination and the phase associated with the dynamics in the ion (both field-free and laser induced). The complexity of the recombination process in the presence of a strong laser field does not enter the interference between the XA and AA channels: recombination with the ion in the A state is identical for both. This interference can be used to record the relative phase of ionization $\phi_{XA} = \phi_A - \phi_X$ into the X and A states of the ion, since the phase associated with the dynamics in the ion can be calculated separately. In the presence of cross-channels, ϕ_{XA} controls the strength of the harmonic emission associated with the recombination with the ion in the excited state $A^2\Pi_u$. We will also show that it controls the ellipticity of emitted harmonics. Systematic measurements of these observables and their comparison with calculations allow us to find ϕ_{XA}.

Since ionization dynamics is strongly dependent on the molecular alignment angle, we need to produce harmonics in aligned molecules and scan the alignment angle. We used the 1-kHz Ti:Sa Aurore laser system at CELIA, providing 8-mJ 35-fs pulses at 800 nm. Our setup is similar to [21]. The laser pulse is split in a pump (molecular alignment) and probe (harmonic generating) pulses with adjustable delay. The two pulses are focused by a 50-cm lens in a 1 mm length pulsed gas jet of N_2 molecules. The focus position is optimized to favor phase matching of the "short" trajectories and filter out the "long" ones [22]. The pump pulse creates a rotational wave packet, with molecules aligned along its polarization every half rotational period ($T_r = 8.4$ ps) [23]. We set the pump-probe delay to 4.1 ps and control the angle Θ between the pump and probe polarizations by rotating a half wave plate. The harmonic radiation is dispersed by a grazing incidence cylindrical grating, imaged on microchannel plates and recorded by a 12-bit CCD camera.

To characterize harmonic polarization, we use a 45° incidence unprotected silver mirror which acts as a polarizer with an extinction ratio around 30. Rotating the polarizations of both the pump and probe beams with a half wave plate is equivalent to rotating the polarizer and produces a sinusoidal modulation of the detected signal, characteristic of a Malus' law [24,25]. The direction of the harmonic polarization is given by the phase of the oscillation, while the degree of ellipticity is determined by the contrast [24]. The measurement requires calibration of the extinction ratio of the polarizer for each harmonic order. We use the measurements at parallel and perpendicular alignment, where the polarization is linear, for calibration. Our experiment cannot distinguish elliptical from partially unpolarized light, which can arise from propagation effects [24]. Hence, we measure an upper bound of the ellipticity. Reference [24] has shown that the deviations were small.

We performed systematic measurements of harmonic spectra and ellipticity vs alignment angle Θ at different laser intensities (Fig. 2). As Θ increases from 0° to 90°, the harmonic intensity monotonically decreases for all harmonics. This behavior is robust against laser intensity variations and is consistent with Refs. [26,27]. The harmonic ellipticity is maximum around $\Theta = 50$–60°, with higher values close to the cutoff at low laser intensity. The signal-to-noise ratio was not sufficient to extract reliable ellipticity values for harmonics above H25. Our results are consistent with [28], even though we measure slightly higher ellipticities. Elliptically polarized high harmonics produced by linearly polarized laser field can result from the anisotropic scattering of the returning electron by the ionic core. In addition, the interference between multiple HHG channels can significantly rotate the main axis of the

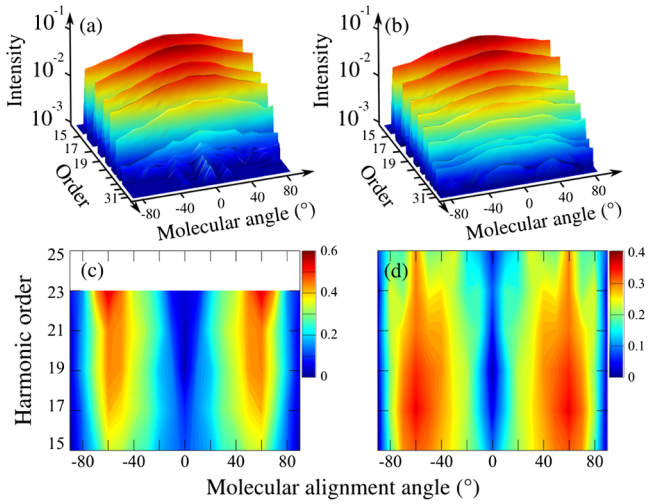

FIG. 2 (color online). Measured harmonic spectra (a),(b) and ellipticity (c),(d) as a function of the molecular alignment angle Θ at $I = 8 \times 10^{13}$ W/cm^2 [(a),(c)] and $I = 1 \times 10^{14}$ W/cm^2 [(b),(d)].

harmonics polarization and create large ellipticities [4]. We take all of these effects into account.

Our theoretical method has been described in [4,5]. Generalizing [29], we write the laser-induced polarization $\mathbf{D}(t)$ (in atomic units) as:

$$\mathbf{D}(t) \propto \sum_{t_b} \sum_{\text{if}} a_{\text{ion},i}(t_b) a_{\text{prop},i}(t, t_b) a_{\text{fi}}^{(N-1)}(t, t_b) \times \langle \Psi^{(N)}(t) | \hat{\mathbf{d}} | \hat{A} \Psi_f^{(N-1)} \chi_f(t, \mathbf{k}(t)) \rangle. \quad (1)$$

Here $\hat{A}$ antisymmetrizes continuum and ionic electrons. The sum over continuum trajectories that start at $t_b(t)$ and recombine at t includes only a single short trajectory, as appropriate for our experimental phase-matching geometry. N-electron wave function $\Psi^{(N)}$ describes the neutral molecule, including quasistatic polarization and depletion by ionization. $\Psi_f^{(N-1)}$ are the $(N-1)$-electron field-free ionic states. Amplitudes $a_{\text{fi}}^{(N-1)}(t, t_b)$ describe laser-induced dynamics in the ion shown in Fig. 1. We include X, A, and B states of N_2^+. In the neutral N_2, the influence of the IR laser field is included quasistatically. Harmonics, calculated by Fourier-transform of Eq. (1), are averaged over model alignment distributions $\cos^4\theta$ and $\cos^6\theta$, with characteristic alignment angles $\sim 30°$ as in experiment.

The propagation amplitude $a_{\text{prop},i}$ between t_b and t is standard (see, e.g., [4,5]). The unknown relative phases of ionization between different channels appear via the complex ionization amplitudes $a_{\text{ion},i}(t_b)$, corresponding to channel i. The absolute values of $a_{\text{ion},i}(t_b)$ are calculated as described in [4,5], including channel coupling by the laser field in the quasistatic approximation. The scattering states χ_f are correlated to the states of the ion $|f\rangle$ and are characterized by the (asymptotic) kinetic momentum $\mathbf{k}(t)$ acquired from the laser field. Here, we use two approaches. The first uses the strong-field eikonal-Volkov approximation (SF-EVA) [30], with scattering on the ion-state specific Hartree potential of the core. The second calculates the laser field-free scattering states using the FERM3D code, as described in [31]. FERM3D naturally includes large-angle scattering absent in SF-EVA, important for describing large ellipticity of the harmonic radiation. Its drawback, common to all field-free stationary scattering calculations, is the contribution of long scattering trajectories trapped near the core for long time, which are not expected to contribute to HHG spectra for short trajectories.

Figure 3 shows results of the calculations. When the initial phase between the ionization amplitudes into the X and A states is set to $\phi_{XA} = 0$, the calculated spectra are very different from the experiment. Setting $\phi_{XA} = \pi$ yields much better agreement. Phases ϕ_{XA} close to π lead to destructive interference of XA and AA channels. In this case, amplitude created in the A state by ionization interferes destructively with the amplitude created in the A state by laser-induced transition from the (polarized) X state after ionization. We performed two sets of calculations, using both SF-EVA and FERM3D approaches. In both cases, the best agreement with experiment is achieved for $\phi_{XA} \simeq \pi \pm 0.2\pi$.

Our approach is similar to Ref. [18], but our results and conclusions are markedly different. The main reason is that we include the subcycle laser-induced dynamics in the ion (absent in [18]), which leads to cross-channels. In particular, channel XA provides very strong signal at $\Theta = 50$–$90°$. Relative ionization phase $\phi_{XA} = 0$ leads to constructive addition of XA and AA channels and higher signal at 90° than at 0°, inconsistent with experiment.

The harmonic ellipticity, which is directly related to the phase properties of the emitted light, should also be very sensitive to ϕ_{XA}. For ellipticity calculations, we use scattering states from the FERM3D code, since SF-EVA underestimates emission with polarization perpendicular to that of the driving field. High values of ellipticity appear already for the sole XX channel due to the structure of the scattering states [Fig. 4(a)]. However, all channels must be taken into account. Then, the shape of the ellipticity map is strongly modified, depending on ϕ_{XA}. Changing ϕ_{XA} from 0 to π changes dramatically its evolution with the har-

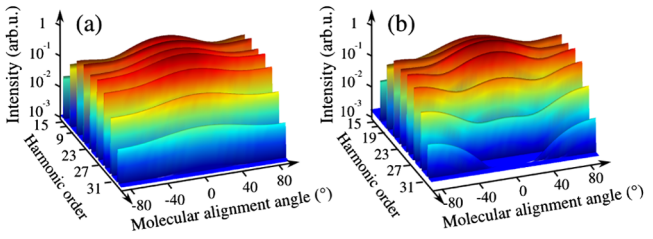

FIG. 3 (color online). Calculated harmonic spectra as a function of molecular alignment angle at $I = 1 \times 10^{14}$ W/cm^2, assuming $\phi_{XA} = \phi_{XB} = \pi$ (a) and $\phi_{XA} = \phi_{XB} = 0$ (b). Results use SF-EVA approach.

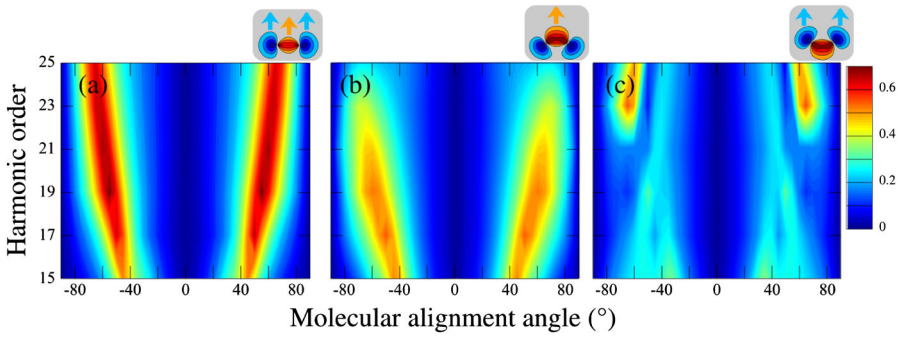

FIG. 4 (color online). Calculated ellipticities as a function of molecular alignment angle at $I = 1 \times 10^{14}$ W/cm^2, with channel XX only (a), all channels and $\phi_{XA} = \pi$ (b) and all channels and $\phi_{XA} = 0$ (c). The insets sketch the corresponding hole minus time-independent background at the instant of ionization, for molecules perpendicular to the laser field. Arrows indicate direction of electron escape. The insets show superposition of the Dyson orbitals (with equal weights), as it is directly related to our measurement [see Eq. (1)] and coincides with the definition of the hole in [10] (in the Hartree-Fock and the frozen-orbital approximation). The multielectron states augmented by the relative phase found in the experiment can also be used to calculate the hole shape following [6,7].

monic order and alignment angle [Fig. 4(b) and 4(c)]. Calculations for intensities between 8×10^{13} W/cm^2 and $I = 1.3 \times 10^{14}$ W/cm^2 give similar results: setting $\phi_{XA} = \pi$ provides good agreement with experiment. These results confirm the value for ϕ_{XA} which was extracted from the harmonic spectra. Our conclusion only applies to $\Theta \sim$ 50–90°, where channels AA and XA are important.

In conclusion, measurements of harmonic spectra and ellipticity allowed us to decode the initial phase between the main ionic states populated by strong-field ionization of N_2. This phase determines the shape and location of the hole created during ionization. Our results suggest that $\phi_{XA} \simeq \pi$, which corresponds to the initial shape of the hole shown in Fig. 4(b) (inset), as opposed to Fig. 4(c) ($\phi_{XA} = 0$) expected in the quasistatic tunnelling limit and in the absence of correlation-induced channel coupling during ionization. We think that the unexpected initial phase reflects unaccounted for electron-electron interaction during ionization, or an intermediate multiphoton resonance in one of the channels. Sensitivity of HH spectra (Fig. 3) and polarizations (Fig 4) to the hole dynamics suggests its control as a route to shaping attosecond pulses.

O. S. and Z. W. acknowledge the Leibniz SAW grant. M. I. acknowledges support of the A. von Humboldt foundation. The CELIA group acknowledges experimental support from D. Descamps, C. Medina, S. Petit, and financial support from the ANR (ANR-08-JCJC-0029 HarMoDyn). We are grateful to the referees for useful comments.

[1] For work prior 2007, see review by M. Lein, J. Phys. B **40**, R135 (2007).
[2] W. Boutu *et al.*, Nature Phys. **4**, 545 (2008).
[3] S. Baker *et al.*, Science **312**, 424 (2006); S. Baker *et al.*, Phys. Rev. Lett. **101**, 053901 (2008).
[4] O. Smirnova *et al.*, Phys. Rev. Lett. **102**, 063601 (2009).
[5] O. Smirnova *et al.*, Nature (London) **460**, 972 (2009); Proc. Natl. Acad. Sci. U.S.A. **106**, 16556 (2009).
[6] S. Lünnemann *et al.*, Chem. Phys. Lett. **450**, 232 (2008).
[7] J. Breidbach and L. S. Cederbaum, Phys. Rev. Lett. **94**, 033901 (2005).
[8] H. Rottke, J. Ludwig, and W. Sandner, J. Phys. B **29**, 1479 (1996).
[9] L. Young *et al.*, Phys. Rev. Lett. **97**, 083601 (2006).
[10] N. Rohringer and R. Santra, Phys. Rev. A **79**, 053402 (2009).
[11] B. K. McFarland *et al.*, Science **322**, 1232 (2008); W. Li *et al.*, Science **322**, 1207 (2008).
[12] H. Akagi *et al.*, Science **325**, 1364 (2009).
[13] S. Haessler *et al.*, Nature Phys. **6**, 200 (2010).
[14] M. Spanner and S. Patchkovskii, Phys. Rev. A **80**, 063411 (2009).
[15] S. Petretti *et al.*, Phys. Rev. Lett. (to be published).
[16] D. A. Telnov and Shih-I Chu, Phys. Rev. A **79**, 041401(R) (2009).
[17] A. T. Le *et al.*, Phys. Rev. A **80**, 013401 (2009).
[18] A. T. Le, R. R. Lucchese, and C. D. Lin, J. Phys. B **42**, 211001 (2009).
[19] M. W. Schmidt *et al.*, J. Comput. Chem. **14**, 1347 (1993).
[20] J. H. Dunning, Jr, J. Chem. Phys. **90**, 1007 (1989).
[21] Y. Mairesse *et al.*, New J. Phys. **10**, 025028 (2008).
[22] P. Salières, A. L'Huillier, and M. Lewenstein, Phys. Rev. Lett. **74**, 3776 (1995).
[23] F. Rosca-Pruna and M. J. J. Vrakking, Phys. Rev. Lett. **87**, 153902 (2001).
[24] P. Antoine *et al.*, Phys. Rev. A **55**, 1314 (1997).
[25] J. Levesque *et al.*, Phys. Rev. Lett. **99**, 243001 (2007).
[26] J. Itatani *et al.*, Nature (London) **432**, 867 (2004).
[27] Y. Mairesse *et al.*, New J. Phys. **10**, 025015 (2008).
[28] X. Zhou *et al.*, Phys. Rev. Lett. **102**, 073902 (2009).
[29] M. Yu. Ivanov, T. Brabec, and N. Burnett, Phys. Rev. A **54**, 742 (1996).
[30] O. Smirnova, M. Spanner, and M. Ivanov Phys. Rev. A **77**, 033407 (2008).
[31] S. Tonzani and C. Greene, J. Chem. Phys. **122**, 014111 (2005); S. Tonzani, Comput. Phys. Commun. **176**, 146 (2007).